

Degradation Mechanisms of a Li-S Cell using Commercial Activated Carbon

Norihiro Togasaki*, Aiko Nakao, Akari Nakai, Fujio Maeda, Seiichi Kobayashi, and Tetsuya Osaka*
Research Organization for Nano and Life Innovation, Waseda University, 513 Waseda-tsurumaki-cho, Shinjuku, Tokyo 162-0041, Japan

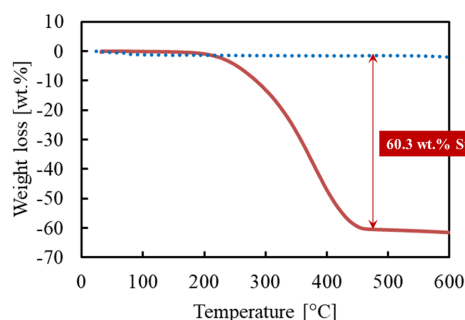


Fig. S1. TGA curves of the S/AC composite with an S/AC weight ratio of 65/35 (w/w). A heating rate of $10^{\circ}\text{C min}^{-1}$ was applied under N_2 . The results revealed that the sulfur mass content of S/AC = 60.3/39.7 (w/w), suggesting that approximately 5 wt.% of sulfur was vaporized as a result of annealing at 300°C for 2 h to remove the additional sulfur from the AC.

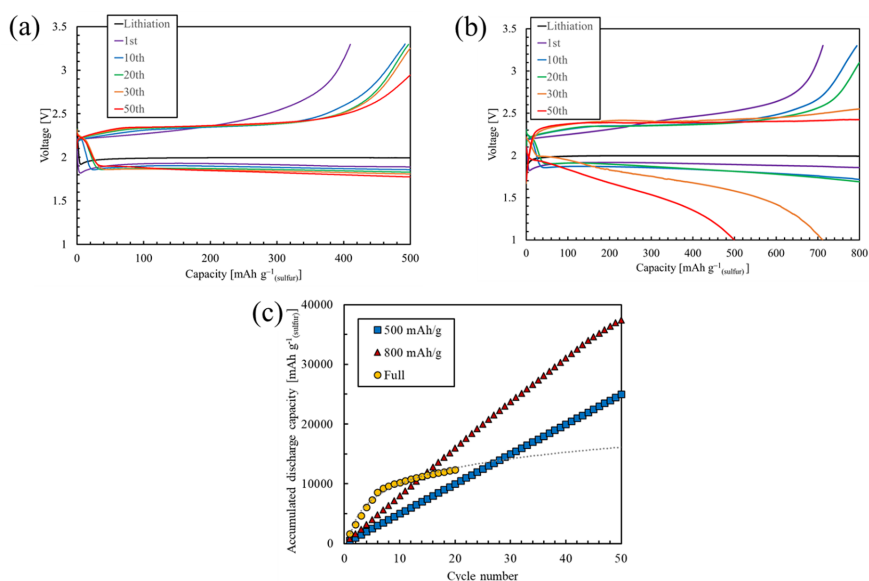


Fig. S2. Lifetime of Li-S cells cycling with limited capacities of (a) 500 mA g^{-1} (sulfur) and (b) 800 mA g^{-1} (sulfur) and the (c) accumulated discharge capacity of Li-S cells cycling with limited capacities of 500 mA g^{-1} (sulfur) and 800 mA g^{-1} (sulfur), and full capacity. Compared to cycling with full capacity, cycling with limited capacities exhibited an advantage in terms of the accumulated discharge capacity, while the accumulated discharge capacity with full capacity cycling leveled off after the 6th cycle and limited capacities prolonged the cycling.

*E-mail address: n-togasaki@ruri.waseda.jp (N. Togasaki), osakatets@waseda.jp (T. Osaka)

DOI: <https://doi.org/10.33961/jecst.2023.00451>

This is an open-access article distributed under the terms of the Creative Commons Attribution Non-Commercial License (<http://creativecommons.org/licenses/by-nc/4.0>) which permits unrestricted non-commercial use, distribution, and reproduction in any medium, provided the original work is properly cited.

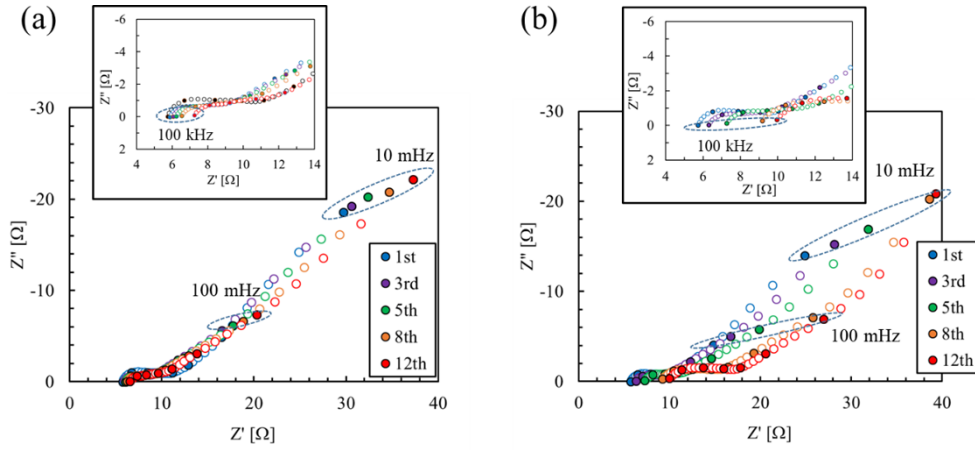


Fig. S3. Nyquist plots for the Li-S cell after discharge at the 1st, 3rd, 5th, 8th, and 12th cycles with a limited capacity for the charge–discharge cycling sequences of (a) 500 mAh g⁻¹ (sulfur) and (b) 800 mAh g⁻¹ (sulfur). In both cases, the impedance increases gradually as cycling progresses. However, each of the impedance signals at an identical cycle number is considerably lower than that in the full charge–discharge sequence in Fig. 3(a).

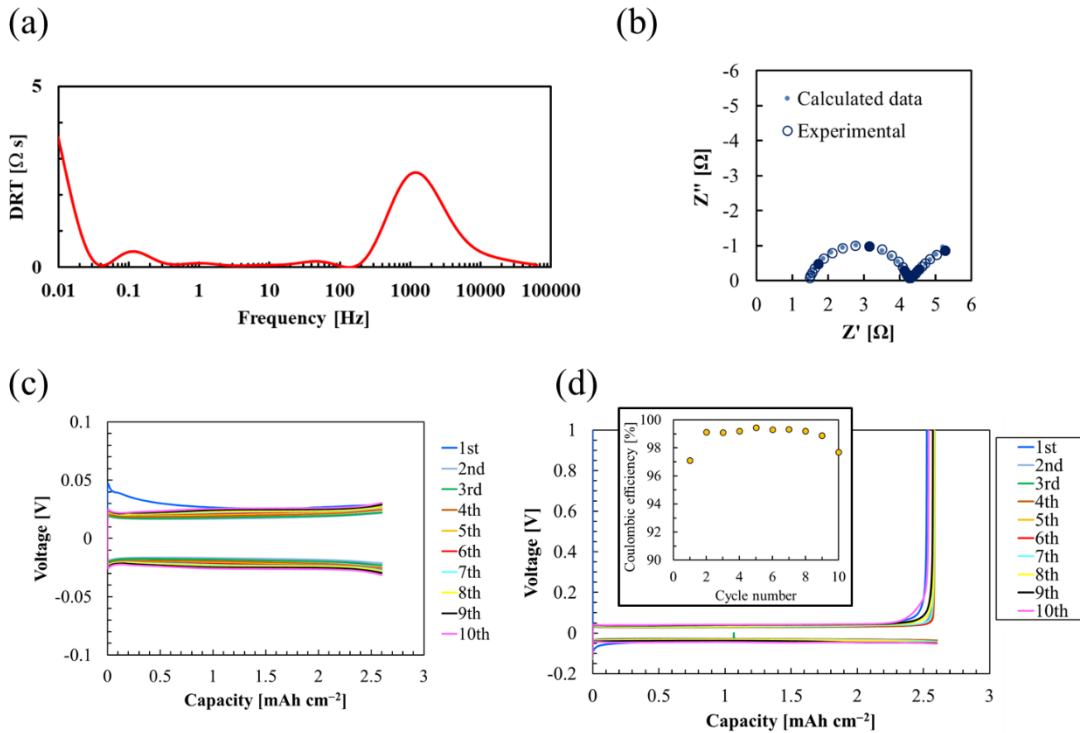


Fig. S4. (a) DRT of the Li/Li symmetrical cell (3×3 cm² lithium metal) after current loading, where the coulombic amount is 2.6 mAh cm⁻² at a current density of 0.26 mA cm⁻². The coulombic amount and current density are similar to those in the lithiation process for a sulfur loading amount of *ca.* 4 mg cm⁻². The fundamental electrochemical process at ~ 1 kHz may be due to the SEI reaction on the lithium surface. (b) Nyquist plots after the abovementioned current loading. The Nyquist plots correspond to reactions of one Li electrode; the obtained Nyquist plots are split in half in the figure. As a result of fitting analysis, the apex frequency, SEI resistance, and interfacial capacitance of SEI are 1.4 kHz, 2.8 Ω and 39 mF, respectively. The obtained apex frequency, SEI resistance and interfacial capacitance of the Li/Li symmetrical cell are identical to those of the Li-S cell shown in Fig. 3. The charge–discharge cycling of the (c) Li/Li symmetrical cell and (d) Li/Cu half-cell.

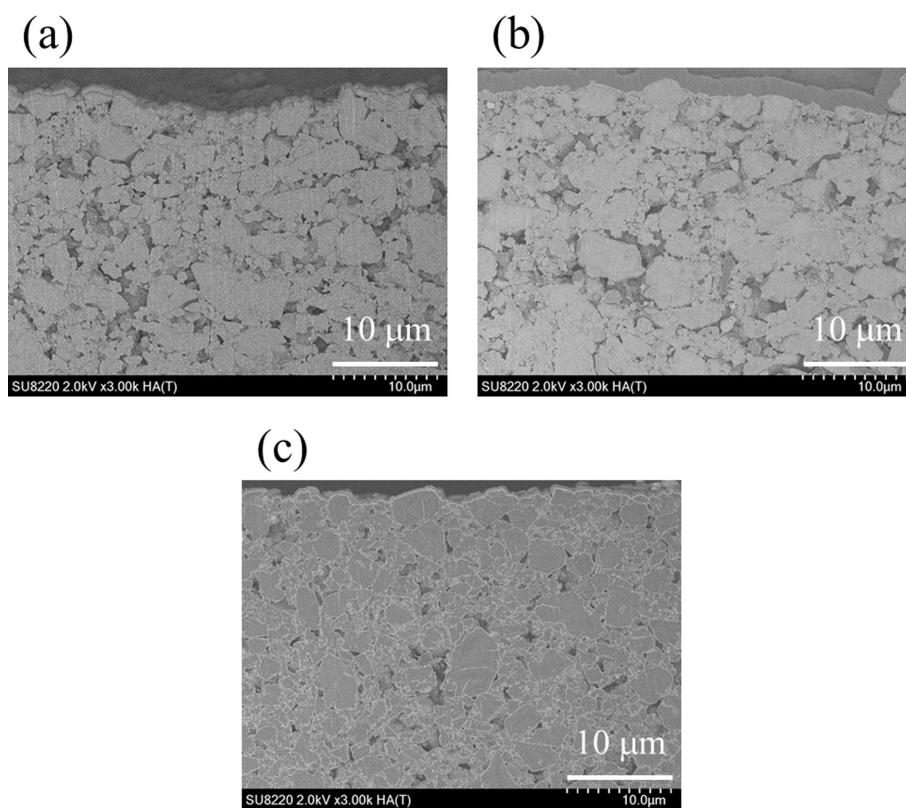


Fig. S5. Cross-sectional SEM images after (a) the lithiation process and after charge–discharge cycling at the (b) 5th cycle and (c) 20th cycle with the full charge–discharge cycling sequence. As cycling progresses, the S/AC cathode composites are observed to be more closely packed, which may be due to the migration of sulfur from inside to outside the AC.